**Table 6**
Mean LAI values measured over several vegetated sites in the *Plaine des Sables* and the *Grand brûlé* in October 2011.

| Studied region | Altitude | Surface characteristics | Mean LAI ($m^2/m^2$) |
|---|---|---|---|
| *Plaine des Sables* | 2310 m | Sparse vegetation (lichen, shrub) | 1.72 ± 0.3 |
| *Grand Brûlé* | 105 m | Tropical forest colonizing the 2002 flow | 2.60 ± 0.5 |
| *Grand Brûlé* | 145 m | Tropical forest colonizing between the 2003 and 2007 lava flows | 7.01 ± 0.2 |
| *Grand Brûlé* | 108 m | Tropical forest near the 2004 lava flow | 7.33 ± 0.4 |
| *Grand Brûlé* | 135 m | Tropical forest colonizing the 2004 lava flow | 8.46 ± 0.4 |
| *Grand Brûlé* | 140 m | Tropical forest colonizing the 2004 lava flow | 9.39 ± 0.6 |
| *Grand Brûlé* | 121 m | Tropical forest colonizing the 2002 lava flow | 9.50 ± 0.6 |
| *Grand Brûlé* | 165 m | Tropical forest colonizing the 2004 lava flow | 9.80 ± 0.5 |

studies (e.g. Duchemin et al., 2006; Steltzer & Welker, 2006) NDVI increases exponentially as a function of LAI and reaches a plateau for values higher than 8 $m^2/m^2$ (Fig. 11). The following model was fit to this scatter plot (Steltzer & Welker, 2006):

$$NDVI = NDVI_{\infty} + (NDVI_{soil} - NDVI_{\infty}) \times e^{-K \times LAI} \quad (14)$$

where $NDVI_{\infty} = 0.9$ is the NDVI of an infinitely-dense canopy (in practice the maximum value found in the image) and $NDVI_{soil} = 0.083$ is the mean NDVI of bare volcanic terrains measured in situ. The extinction coefficient $K = 0.31$ was fitted by model inversion.

Finally, LAI is easily inferred from Eq. (14).

$$LAI = \frac{-1}{0.31} \times \ln\left(\frac{0.90 - NDVI}{0.82}\right). \quad (15)$$

To study the influence of vegetation density on interferometric coherence loss, we generated a LAI map with 25 m spatial resolution using Eq. (15) and compared it with the coherence map calculated from two PALSAR images acquired on Jul. 28, 2010 and Sept. 12, 2010 in HH polarimetric mode (Fig. 6.d). Fig. 12 shows the relationship between LAI and radar coherence. One clearly observes that coherence linearly decreases with LAI. We calculated the regression line as:

$$\gamma_{HH-HH} = -0.054 \times LAI + 0.96. \quad (16)$$

This relationship, which is derived for the first time in this paper, highlights the sensitivity of InSAR signals to vegetation density. We use it to propose a threshold, LAI = 7.5, over which deformation measurements are altered and become unreliable in L-band.

## 7. Conclusions

This work definitely improves our understanding of spatial and temporal variations in L-band InSAR coherence arising from textural changes as measured using LiDAR. Our cross-relation study mixes ALOS/PALSAR coherence images, airborne LiDAR data, and LAI and GPR field measurements acquired over the *Piton de la Fournaise*. The main conclusions that can be drawn are twofold: (1) LiDAR data provided very detailed elevation maps of the *Piton de la Fournaise* in 2008 and 2009. They permitted the estimation of the lava volume emplaced on the Dolomieu crater floor, which explains the temporal variation of the interferometric coherence observed over the main crater. (2) The analysis of normalized intensity LiDAR allowed us to identify different volcanic products and vegetation covers because of their spectral signature, and hence contributed to the understanding of the link between InSAR coherence and terrain type. To sum up, dense vegetation in the *Grand Brûlé* and outside the caldera produces significant temporal decorrelation. Region covered by lapilli or a′a lava flows also induce decorrelation whereas pahoehoe lava flows have good coherence. We also investigated the dependence of InSAR coherence on surface roughness, microwave dielectric properties of rocks and vegetation density. Such studies allowed us to discriminate between scattering and volumetric effects: we observed high coherence loss over rough a′a lava flows caused by radar wave multiple scattering and over pyroclastic deposits caused by radar wave penetration into the medium. Over veg-

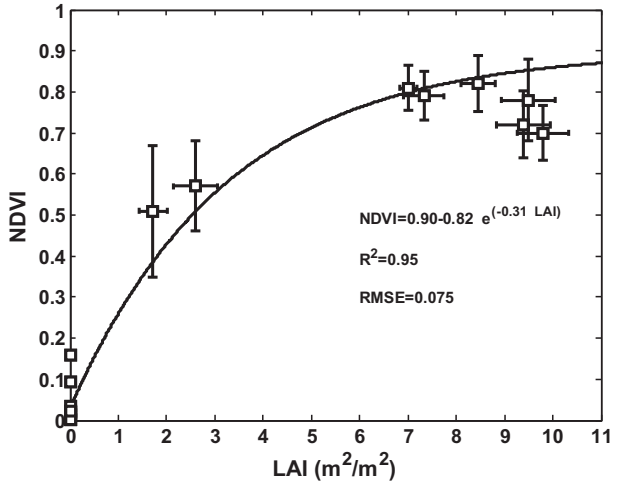


**Fig. 11.** LAI–NDVI relationship. Symbols are centered on field-averaged LAI and NDVI values. Horizontal and vertical bars show the LAI and the NDVI standard deviations, respectively. The five points at LAI = 0 correspond to bare ground (lava flows, lapilli deposits).

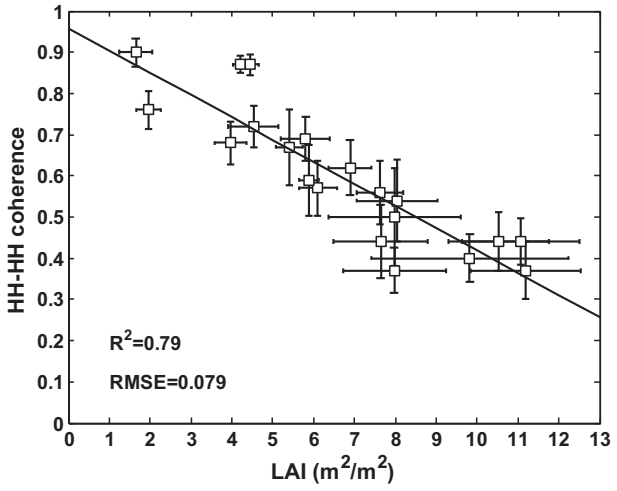


**Fig. 12.** Correlation between LAI and InSAR coherence in HH polarization. Symbols are centered on field-averaged LAI and coherence values. Horizontal and vertical bars show the LAI and the coherence standard deviation, respectively.